Chemical Physics Letters 789 (2022) 139298

Contents lists available at ScienceDirect

Chemical Physics Letters

journal homepage: www.elsevier.com/locate/cplett

Computational investigation on potential energy surface evolution: The tautomerization from enediyne to enyne-allene

Hailong Ma, Mengsi Zhang, Yaxian Zhang, Aiguo Hu, Yun Ding *

Shanghai Key Laboratory of Advanced Polymeric Materials, School of Materials Science and Engineering, East China University of Science and Technology, Shanghai 200237, China

ARTICLE INFO

Keywords:
Enediyne
Proton transfer
Enyne-allene
Charge separated intermediate
Potential energy surface

ABSTRACT

1,3-proton transfer process is investigated theoretically on enediyne system with the help of different non-metallic catalysts. By tuning the substituents at the ene site and carefully selecting the catalyst, it is possible to manipulate the potential energy surface, where the reaction mechanism can be converted from fully concerted one, to "hidden transition state" concerted mechanism, and finally in a stepwise manner. Natural bond orbital interactions have revealed that the reaction mechanism is determined by the stability of the charge separated intermediate after deprotonation, where the interplay of the negatively charged substrate and the protonated catalysts plays the vital role.

1. Introduction

Proton transfer process is ubiquitous in chemical and biochemical related events, such as the migration of hydronium ion in liquid water [1–6], intramolecular proton transfer in amino acids [7,8] and DNA [9–12], not to mention the C—H activation [13,14] involved in numerous organic reactions. Consequently, such processes are extensively investigated both experimentally [13–18] and theoretically [4–6,9,10,12–20]. In particular, tautomerization is a class of reactions achieved through intramolecular proton transfer, which is responsible for DNA mutation [9–11], for instance. However, direct intramolecular proton transfer is a rare event at room temperature due to their high reaction barrier [20]. Acids [21], bases [19,20,22], and solvents such as water or alcohol [19,23–25] are generally applied as proton shuttles in the investigation of indirect intramolecular proton transfer in order to lower the reaction barrier [26,27]. To this end, in-depth understanding of the reaction mechanism and possible ways to manipulate the potential energy surface is of great importance [28,29], which could help us to control the reaction and guide us to better design the substrates and catalysts.

One important application of proton transfer is the tautomerization of propargyl group in enediynes (EDYs), a class of compounds with alternating C—C double and triple bonds. Such compounds with this unique core moiety have demonstrated great anticancer potential for a broad cancer cell lines since their first discovery from natural products [30,31]. Their high antitumor ability stems from the biradical intermediates generated from Bergman cycloaromatization (BC, Scheme 1) [32–34], which is accountable for the reactivity of a group of natural enediynes, like calicheamicin [35]. However, such mechanism is energetically demanding in general and requires high reaction temperature [36], which is disadvantageous for experimentally easy-to-synthesize acyclic enediynes. Alternatively, biradicals can be generated through Myers-Saito cycloaromatization (MSC, Scheme 1) [37–39] from their correspondent enyne-allene isomers, which show accessible reaction barriers at physiological temperature. Recently, our group uncovered a new reaction mechanism called maleimide-assisted rearrangement and cycloaromatization (MARACA), where the electron-deficient maleimide moiety at the ene position of enediynes is found to facilitate the proton transfer processes [21]. As a result, acyclic enediynes with relatively simple structures are able to generate diradical at room temperature and show high cytotoxicity towards a panel of cancer cell lines [21].

Intrigued by these findings, 1,3-proton transfer process was investigated by means of density functional theory (DFT), as it was the critical and least step to realize the conversion from enediyne to enyne-allene. The potential energy surfaces (PES) of 1,3-proton transfer were examined carefully for enediynes with bulky substituents installed at the yne sites with the assistance of different catalysts. Our findings reveal that the shape of the potential energy surface is determined by the interplay of the substrate and the catalyst, whose ability to accommodate the extra charge in the charge separated intermediate after proton abstraction is

* Corresponding author.
E-mail address: yunding@ecust.edu.cn (Y. Ding).

https://doi.org/10.1016/j.cplett.2021.139298
Received 18 October 2021; Received in revised form 2 December 2021; Accepted 17 December 2021
Available online 23 December 2021

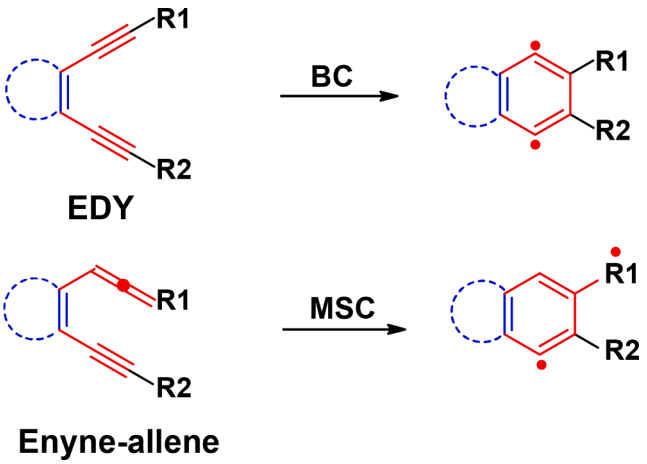

Scheme 1. Bergman and Myers-Saito cyclization reactions.

crucial for the reaction mechanism, i.e., concerted or stepwise. By stabilizing the charge separated intermediate, it is possible to convert the reaction mechanism from concerted to stepwise manner, and lower the reaction barrier as well.

2. Computational methods

All the calculations were carried out in Gaussian 09 [40] package. The structures were optimized first at the computational level of B3LYP/6–31G* in gas phase, which has been demonstrated accurate enough to elucidate the reaction mechanisms in similar systems in our previous work [21,41,42]. Meanwhile, further structure optimizations were performed in the implicit solvent of water (ϵ=78.3553) with the conductor-like polarizable continuum model (CPCM) [43,44] implemented in the self-consistent reaction filed (SCRF) approach at B3LYP/6-31+G* or B3LYP/6-311+G* level. Grimme's D3 dispersion correction [45] was included in all calculations. All the reactants, transition states (TSs), intermediates and the products of different 1,3-proton transfer reactions were successfully characterized using harmonic vibrational frequency analysis in the ambient condition and the optimized structures were verified to be either minima (with no imaginary frequency) or TSs (with only one imaginary frequency). The intrinsic reaction coordinates (IRC) calculations [46] were carried out in gas phase to confirm the reaction pathways and to obtain the potential energy curves. For TSs optimized in water phase, IRC calculations were performed for the four systems depicted in Fig. 5 at B3LYP/6-311+G* level in order to make a comparison, while the vibrational mode corresponding to the imaginary frequency was check for the rest TSs in water phase, which suggested identical vibrational modes as the TSs in gas phase except the maleimide-based EDY catalysed by water, which was further confirmed through IRC calculation.

The obtained energies are reported in ΔE, ΔG, and $\Delta G^{\#}$, representing the relative electronic energy (without zero-point energy correction), relative Gibbs free energy, and the activation free energy, respectively.

Natural bond orbital (NBO) [47–50] interactions were evaluated based on the optimized structures with B3LYP/6–31G(d) using NBO 3.1 [51] module embedded in Gaussian09 [40], where strictly localized orthogonal orbitals were generated. In NBO analysis, the second order perturbation theory was employed to estimate the orbital donor–acceptor interactions. The structures and orbitals presented in this work were generated using VMD [52], and Multiwfn [53].

3. Results and discussion

3.1. Different catalysts play an important role during 1,3-proton transfer

EDYs have the ability to generate diradicals, which is crucial to kill cancer cells. However, to widely apply them in chemotherapy, it requires the EDYs to have an easy-to-synthesize structural design and the ability to undergo cyclization reactions at physiological temperature. The conversion of EDY to enyne-allene is critical to trigger the low reaction barrier MSC mechanism instead of the high barrier BC mechanism. Such conversion could be achieved through 1,3-proton transfer, which has been demonstrated a promising strategy [21].The process of proton transfer involves the abstraction and the addition of a hydrogen cation. Generally, the strong σ-bonding C—H bond is hard to dissociate without the help of an external catalyst. Thus, the strong bases, such as 1,8-diazabicyclo[5.4.0]undec-7-ene (DBU) [21,22,54] and 1,5,7-triazabi-cyclo[4.4.0]dec-5-ene (TBD) [54], are selected as catalysts to accelerate the proton transfer process. Besides, ubiquitously available H_2O and acids like CH_3COOH are found to promote the proton transfer process as well. Here, the 1,3-proton transfer process is investigated in detail with the help of five kinds of catalysts: $H_2PO_4^-$, 1,4,6,9-tetraaza-5l5-phosphaspiro[4.4]non-1(5)-ene (NPN), H_2O, CH_3COOH and $N(CH_3)_3$ (Scheme 2). EDYs with bulky substituents installed at the alkynyl termini were employed in the following calculations, where the electron-withdrawing group will further boost the C—H dissociation. Depending on the substituents at the ene position, the ethylene-, benzene-, and maleimide-based EDYs are denoted as **R1**, **R2** and **R3**, respectively (Scheme 2). These structures are proved easy-to-synthesize experimentally and the maleimide-based ones showed relatively high cytotoxicity towards a panel of cancer cell lines [21]. The Gibbs free energy barriers at ambient condition are summarized in Table 1, and most of the chosen catalysts could be found in the biological environment.

Depending on the substrate and the chosen catalyst, the investigated 1,3-proton transfer follows the concerted or stepwise mechanism. The strongest base in the group, NPN, proposed by Alabugin et al. [54], shows the ability to assist the proton transfer process in a stepwise manner at room temperature regardless of the substrates (highest activation free energy of 21.1 kcal/mol). Taking **R1** for example, the complex **R1*** was first formed by **R1** and NPN, then NPN abstracted the proton at C1 position through **TS1-R1**, forming a stable intermediate **INT1**, after that one proton was released to C3 position through a transition state of **TS2-R1**, forming the enyne-allene product **P1** at last (Fig. 1). The rate-determine steps in the NPN involved cases are the cleavage of the C—H bond except **R3**, where the reaction intermediate **INT3** is more stable compared to the reactant, as a result, the rate-determine step shifts to proton addiction. On the contrary, in the presence of CH_3COOH or H_2O, all the reactions go through a concerted mechanism, where the activation Gibbs free energies are much higher compared to the ones in the presence of NPN and the reactions are difficult to occur at physiological temperature (Table 1). Interestingly, the water wire formed by three water molecules could significantly lower the reaction barrier, 36.0 vs. 51.4 kcal/mol when a single water molecule acts as the catalyst indicated by the results calculated in gas phase. Such phenomena are also observed in the proton or hydrogen atom transfer process related to other reaction environments [55,56]. Both single water molecule and the water wire could accept and donate a proton in a concerted manner. The significant effect of the number of water molecules on the reaction barrier might be related to the matching distances between the two oxygen atoms in the water wire and the underneath C1-C3 in the substrate, which stabilize the TS. $N(CH_3)_3$ would prefer to work in a stepwise manner due to its structural limitation as it cannot serve as proton donor and acceptor simultaneously. The ability of working as proton donor and acceptor simultaneously is vital for concerted 1,3-proton transfer. Although tremendous effort was devoted to the **R2** systems, we could not find the TS corresponding to the

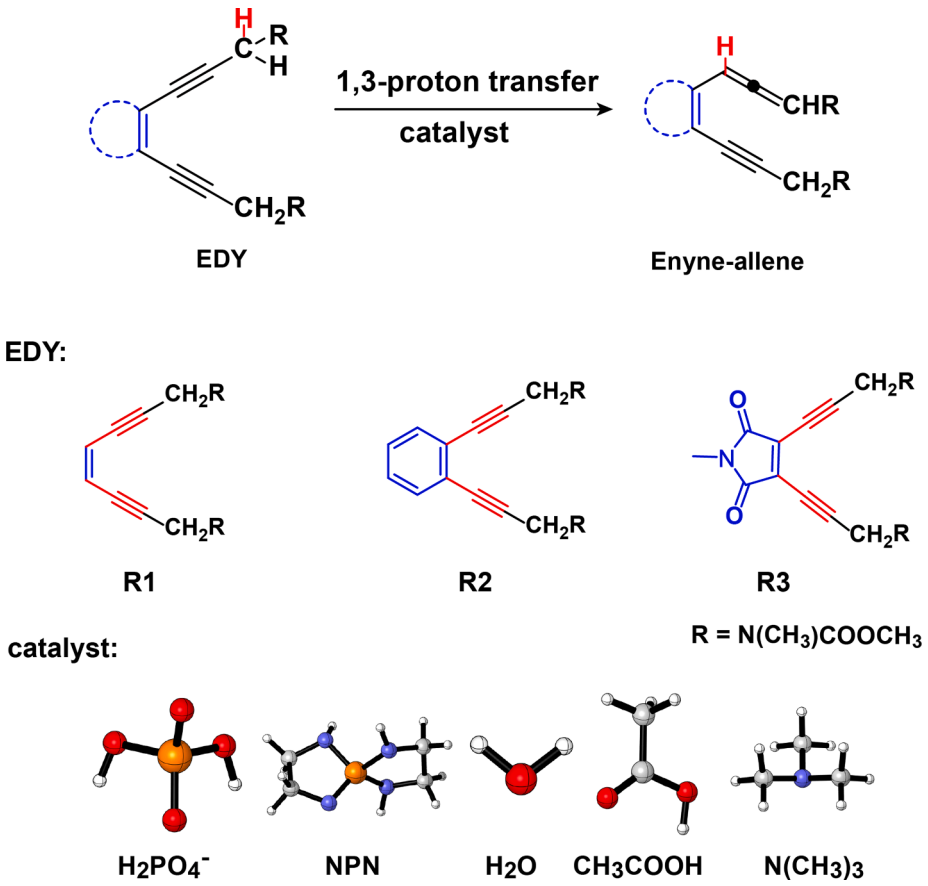

Scheme 2. EDY systems employed in the calculations with different catalysts.

Table 1
Gibbs free energy barriers for 1,3-proton transfer in EDYs with the help of different catalysts at 298.15 K (in kcal/mol).

	R1		R2		R3	
	$\Delta G_1^{\#a}$	$\Delta G_2^{\#b}$	$\Delta G_1^{\#}$	$\Delta G_2^{\#}$	$\Delta G_1^{\#}$	$\Delta G_2^{\#}$
NPN	15.8[c]	−0.4[d]	14.9	0.8	8.8	11.4
	(20.0)[e]	(4.8)	(21.1)	(3.2)	(11.5)	(20.1)
$H_2PO_4^-$	21.0		14.9		10.0	6.2
	(34.2)		(33.8)		(24.2)	(7.8)
	[34.6][f]		[34.1]		[24.6]	[9.1]
$N(CH_3)_3$[g]					17.6	3.9
					(17.3)	(6.6)
CH_3COOH	34.8		33.9		36.6	
	(39.4)		(39.3)		(38.5)	
					[39.7]	
H_2O	52.4		49.3		51.4	
	(60.7)		(53.8)		(51.6)	
water wire ($3H_2O$)					36.0	

[a] Gibbs free energy barrier for TS1. In concerted reaction manner, only one TS is present, while for stepwise 1,3-proton transfer, this corresponds to the proton abstraction step. [b] Gibbs free energy barrier for TS2, which corresponds to proton addition in stepwise 1,3-proton transfer. [c] Calculated at B3LYP-D3/6–31G* in gas phase. [d] The electronic energy of the TS is 0.8 kcal/mol higher than the intermediate. The negative activation free energy barrier comes from the entropic contribution. [e]Energies in parenthesis are calculated at B3LYP-D3/6-31+G* in CPCM model of water. [f] Energies in square brackets are calculated at B3LYP-D3/6-311+G* in CPCM model of water. [g] Despite of tremendous efforts, we could not locate the TS of proton abstraction in stepwise 1,3-proton transfer for **R2**.

stepwise proton transfer with the help of $N(CH_3)_3$. The charged $H_2PO_4^-$ seems to facilitate the proton transfer in **R3** at room temperature, considering the relatively low reaction barriers (24.6 and 9.1 kcal/mol in water phase), which is in consistent with the experimental findings, where the maleimide-based EDY could successfully generate radical species at room temperature, while the benzene-based one failed [21]. Despite of the height of the reaction barrier, the substrates start to play a role in the reaction mechanism. The 1,3-proton transfer in **R3** catalyzed by $H_2PO_4^-$ still shows a stepwise mechanism, while in **R1** or **R2**, the reactant complex **R2*** or **R4*** goes through the transition state of **TS-R1** or **TS-R2** respectively to achieve the final enyne-allene product **P1** or **P2** (Fig. 1).

In general, for **R3**, the 1,3-proton transfer tends to go through stepwise mechanism with the help of a strong base, while in the presence of a weak base which could serve as a proton shuttle, concerted mechanism is observed with a much higher reaction barrier. The only exception is $H_2PO_4^-$, where stepwise reaction mechanism is preferred in the presence of the relatively weak base. However, for **R1** and **R2**, only the strongest base examined in this work, i.e., NPN, could stabilize the reaction intermediate, in another words, the reaction is stepwise.

3.2. Revealing the mechanism of proton transfer

3.2.1. The potential energy surfaces in gas phase

Up till now, it is clear that two kinds of reaction mechanisms, concerted and stepwise, are possible in the proton transfer process of EDYs. Although the specific reaction investigated in this work is conducted in solvent, potential energy surfaces in gas phase allow us to have a better understanding on how the substrate and the catalyst affect the reaction mechanism from a simpler picture, without the influence of solvation effect. IRC calculations revealed that the potential energy

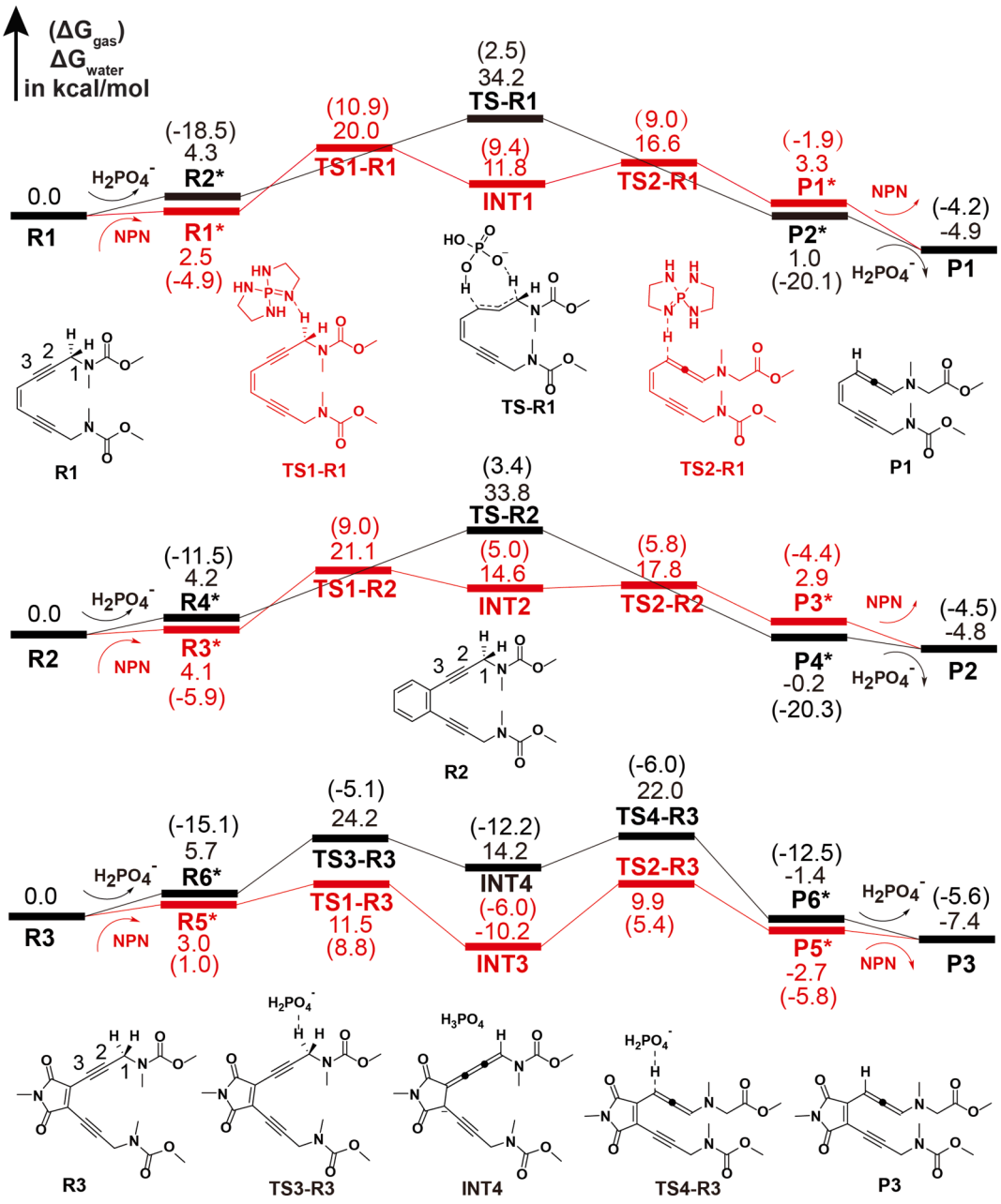

Fig. 1. Gibbs free energy profiles of **R1**,**R2** and **R3** catalyzed by NPN or $H_2PO_4^-$.

surfaces (PES) were in three different shapes (Fig. 2), which are denoted as concerted proton transfer, where proton abstraction and addition take place synchronously, "hidden-TS" concerted proton transfer, which corresponds to the partial overlap of the independent proton abstraction and addition PES, and stepwise proton transfer (Fig. 2). The proton abstraction step will generate a negatively charged EDY ion (denoted as EDY-p) and a catalyst with an extra proton (denoted as CAT+p,where +/-p indicates adding or minus one proton). The intermediate could be considered as a complex formed by EDY-p and CAT+p, i.e., a charge separated system, whose stability actually relies on the stability of each component and largely determines the shape of the PES. Taking CH_3COOH for example, the addition of an extra proton will destabilize the structure in a large extent, thus the deprotonation of the originally bonded H atom has to occur simultaneously (Figure S2A). In the TS, both OH distances are much longer compared to that of an OH bond, 1.32 and 1.27 Å (Fig. 2E), preparing for the formation of O-H1 in CH_3COOH and C3-H2 in the substrate respectively. As a result, the process of proton transfer is completed in a fully concerted mode (Fig. 2A). On the contrary, $H_2PO_4^-$ could stabilize the extra proton, thus the protonation and the deprotonation of the catalyst are possible to become independent incidents. In this case, the stability of EDY-p is accounted for the stepwise behaviour. If we take the middle point of TS and the hidden-TS along the reaction coordinate as the charge separated structure in "hidden-TS" concerted proton transfer (MP-R1 in Fig. 2B and MP-R2 in Fig. 2C), which is similar to the intermediate in a stepwise proton transfer (INT4 in Fig. 2D), we could conclude from the PES that **R3** has the strongest ability to accommodate the extra electron, while **R1** the weakest. As compared to the TS, the energy of the middle point (MP-R1) decreased by only 0.6 kcal/mol. The instability of the charge separated structure is the driving force to lower the energy of the second TS, leading to the "hidden-TS" concerted mechanism [54]. The ability of the substrate to accommodate the extra charge is indicated by the delay of the second TS compared to the first one, where the weakest substrate, i.e., **R1**, has the shortest delay appeared in the PES (Fig. 2B). The plateau

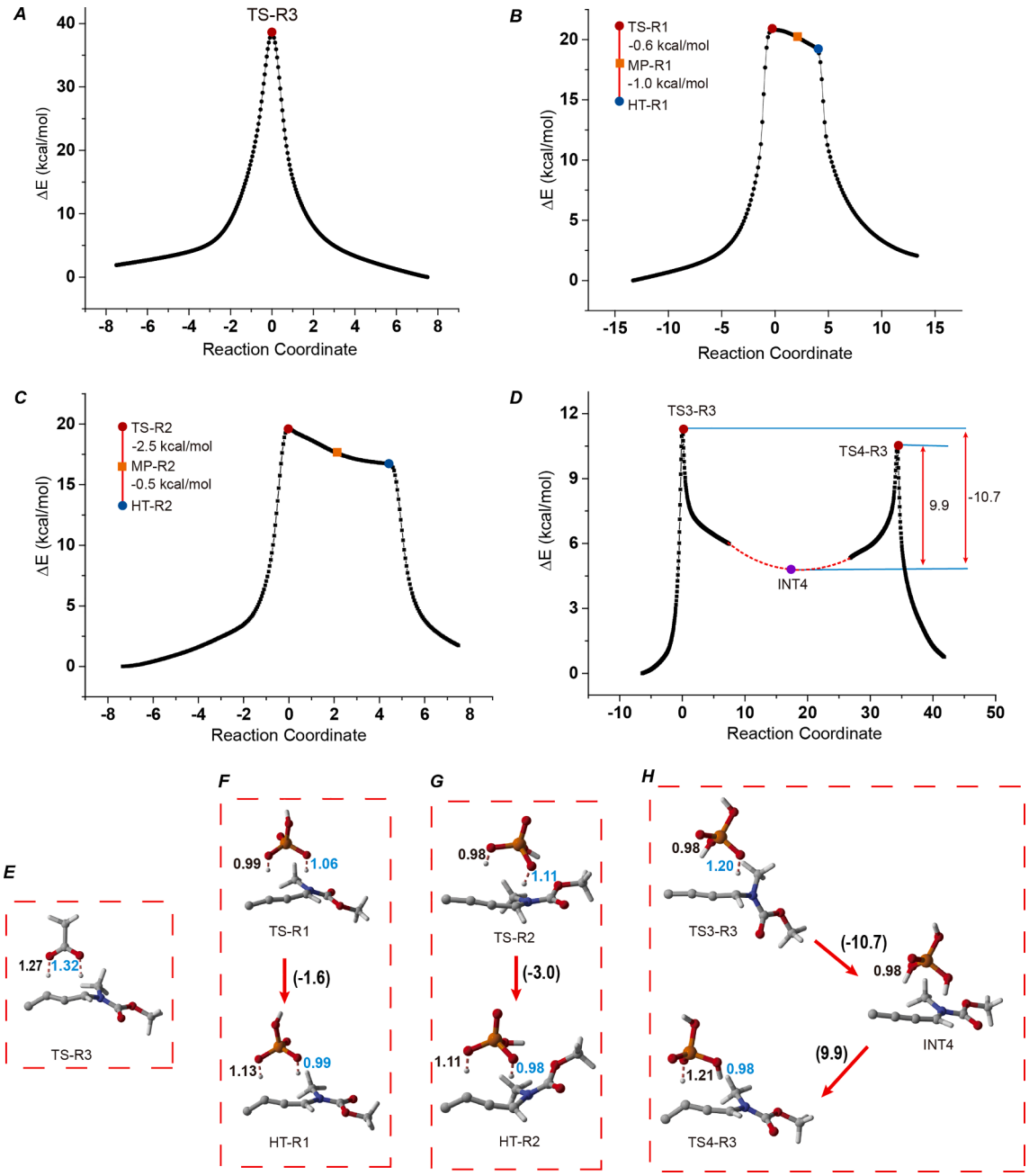

Fig. 2. 1,3-proton transfer potential energy curves and the corresponding structures of **R3** + acetic acid (A and E), **R1** + $H_2PO_4^-$ (B and F), **R2** + $H_2PO_4^-$ (C and G), and **R3** + $H_2PO_4^-$ (D and H) obtained in gas phase. The black lines in the PES are from IRC calculations starting from the TSs as indicated by red solid circles. The "hidden-TS" are labelled by blue solid circles, while yellow squares indicate the middle point (MP) of TS and the hidden-TS in each PES. Only the reactive sites are shown in the structures with P in orange, N in blue, O in red, C in gray, and H in white. The OH distance in blue represents the proton for abstraction, while the OH distance in black represents the proton for addition (units in Å). The numbers in the parenthesis along the red arrows represent the relative single-point energies corresponding to the PES (units in kcal/mol).

area in the PES is reflected on the OH distance profile along the reaction coordinate as well (Figure S2B and C). For both **R1** and **R2**, a range of reaction coordinates indicating both OH distances around 1.0 Å is observed, which corresponds to the catalyst fully accepting the proton. The O-H2 bond breaking is delayed compared to the bond formation of O-H1.

Fig. 2 provides a picture of the potential energy surface evolution depending on both the substrate and the catalyst, where the intricate interplay of the charge separated structure after proton abstraction plays an important role. By further stabilization the charge separated intermediate, it is possible for the reaction in stepwise mechanism to abort after proton abstraction. As mentioned above, the stabilization of **INT3** shifted the rate-determine step from proton abstraction to proton addition.

3.2.2. *The stability of EDY after proton abstraction*

Since the stability of the charge separated intermediate after proton abstraction is critical to the reaction mechanism, we will first look at the stability of EDY after loosing one proton, which helps to understand how the shape of the PES changes in the presence of the same catalyst. Table S1 shows the Wiberg bond indices of C—C bonds in EDY anions after proton abstraction. Clearly, the presence of the benzene and maleimide rings helps to delocalize the extra electron, where the triple bonds are severely weakened.

To have a better understanding of how the negative charge is stabilized in the substrate after proton abstraction, we turn to the NBO interactions based on the second-order perturbation theory. The NBO orbitals usually describe strictly localized Lewis structures. The interactions between a filled NBO orbital and an unfilled NBO orbital, such as the antibonding orbital, represents the deviation from the localized Lewis structure, which is considered as a measure of molecular delocalization and is beneficial for molecular stabilization [29]. In the case of EDY-p anions, we are interested in the carbon lone pair (LP) orbital, which represents the position of the unbonded electrons. The strong orbital–orbital interactions with carbon LP serving as the donor are depicted in Fig. 3. To our surprise, in the ground state, the stable resonance structure has the carbon LP orbital locating at the C5 position instead of the reactive site of proton addition, i.e., the C3 position, which indicates that the deprotonated EDY structures will go through a charge transfer process and result in a buta-1,2,3-triene (C═C═C) structure. As a result, the double bond in the original EDY has to break, which will destroy the aromaticity of the benzene ring and is disadvantageous to **R2**-p. Without the existence of extra conjugated rings, the charge in carbon LP can only be stabilized by nearby π^*(C—C) in **R1**-p (Fig. 3A). Extra stabilization of π^*(C—C) in the benzene ring is suggested from the NBO results (Fig. 3B). The strongest delocalization effect comes from the maleimide ring, where the adjacent electron-withdrawing C═O bond shows the strongest delocalization ability (Fig. 3C, 118.9 kcal/mol.) The calculated interaction energies are too large for second-order perturbation theory, however, it could be considered as a measure for the stabilization abilities among different EDY-p [29]. The calculated orbital–orbital interaction energies help to understand how the negative

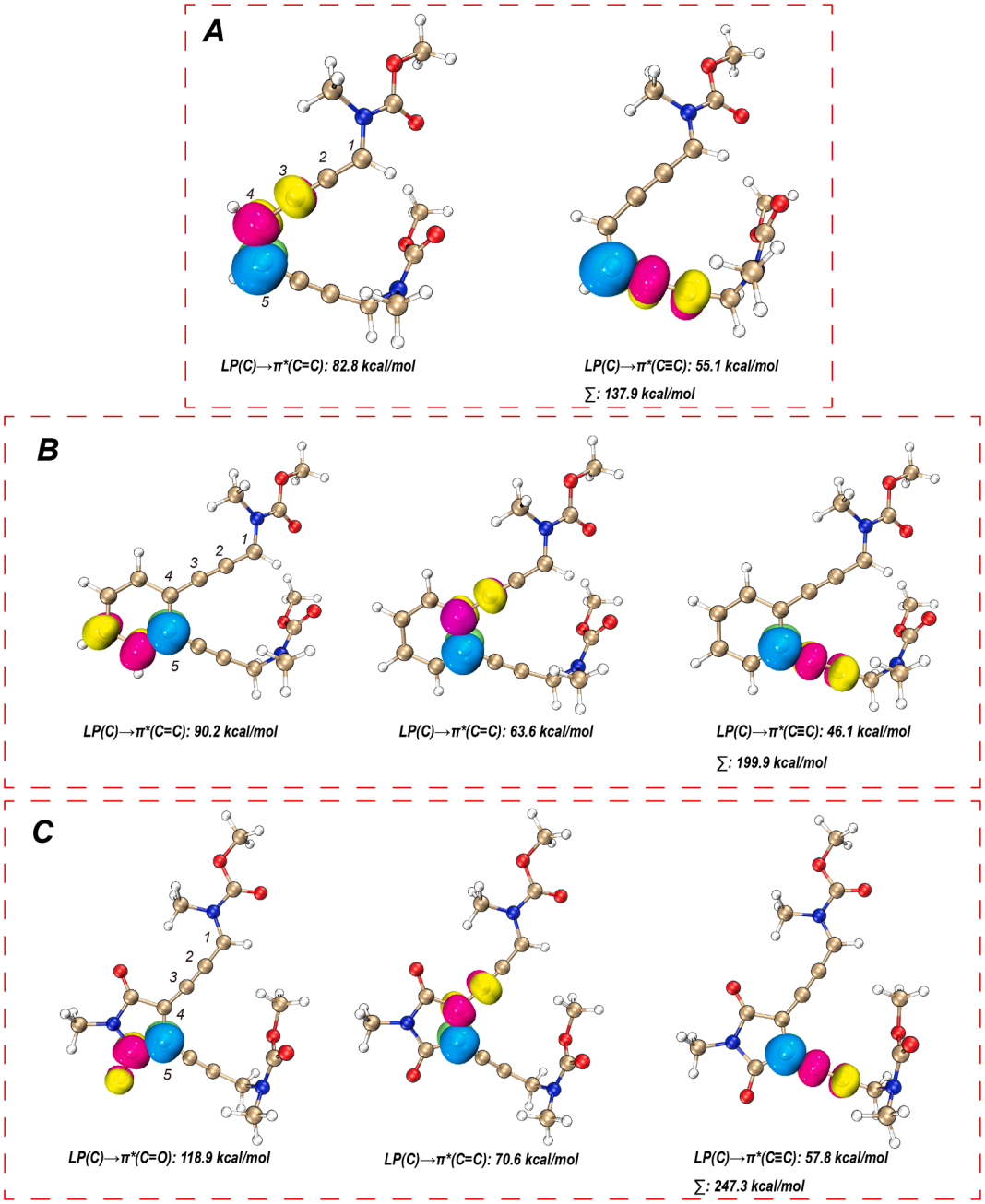

Fig. 3. NBO interactions between the carbon lone pair (in cyan and green) and the antibonding orbitals (in magenta and yellow) in the optimized substrates after deprotonation. (A). **R1**; (B). **R2**; (C). **R3**. The color code for atomic kinds is C in golden, N in blue, O in red and H in white. Σ represents the sum of all the interactions in each system. The orbitals are generated at the density of 0.08 a.u.

charge was stabilized after proton abstraction in each substrate, meanwhile, the values of the interaction energies could provide the stability order of the three substrates investigated. In summary, the maleimide moiety has the strongest ability to delocalize the charge density (NBO interactions of 247.3 kcal/mol in total), while the **R1** has the weakest ability (NBO interactions of 137.9 kcal/mol in total) due to the lack of substituent at the ene position. In all three systems, only **R3**-p can exist free-standing as we will show later. In this case, the delocalization of the carbon LP orbital to the π^* orbital at the C3 position provides reactivity for 1,3-proton transfer.

The stabilization ability of different EDY-p to the extra charge could explain the potential energy surface evolution in the presence of the same catalyst, such as the case of $H_2PO_4^-$. However, to gain insights on how different catalysts change the reaction mechanism of the same substrate, we have to look deeper at the charge separated intermediate. Fig. 4 shows the NBO interactions of the optimized reaction intermediates in the presence of a catalyst. The strongest base in the investigated group, NPN, is chosen, as it demonstrates the ability to interrupt the proton transfer process into a stepwise manner regardless of the substrate. In **R3**, the binding between the deprotonated substrate and the protonated NPN is mainly van der Waals interactions, as no direct orbital–orbital interaction was observed (Fig. 4C). The carbone LP

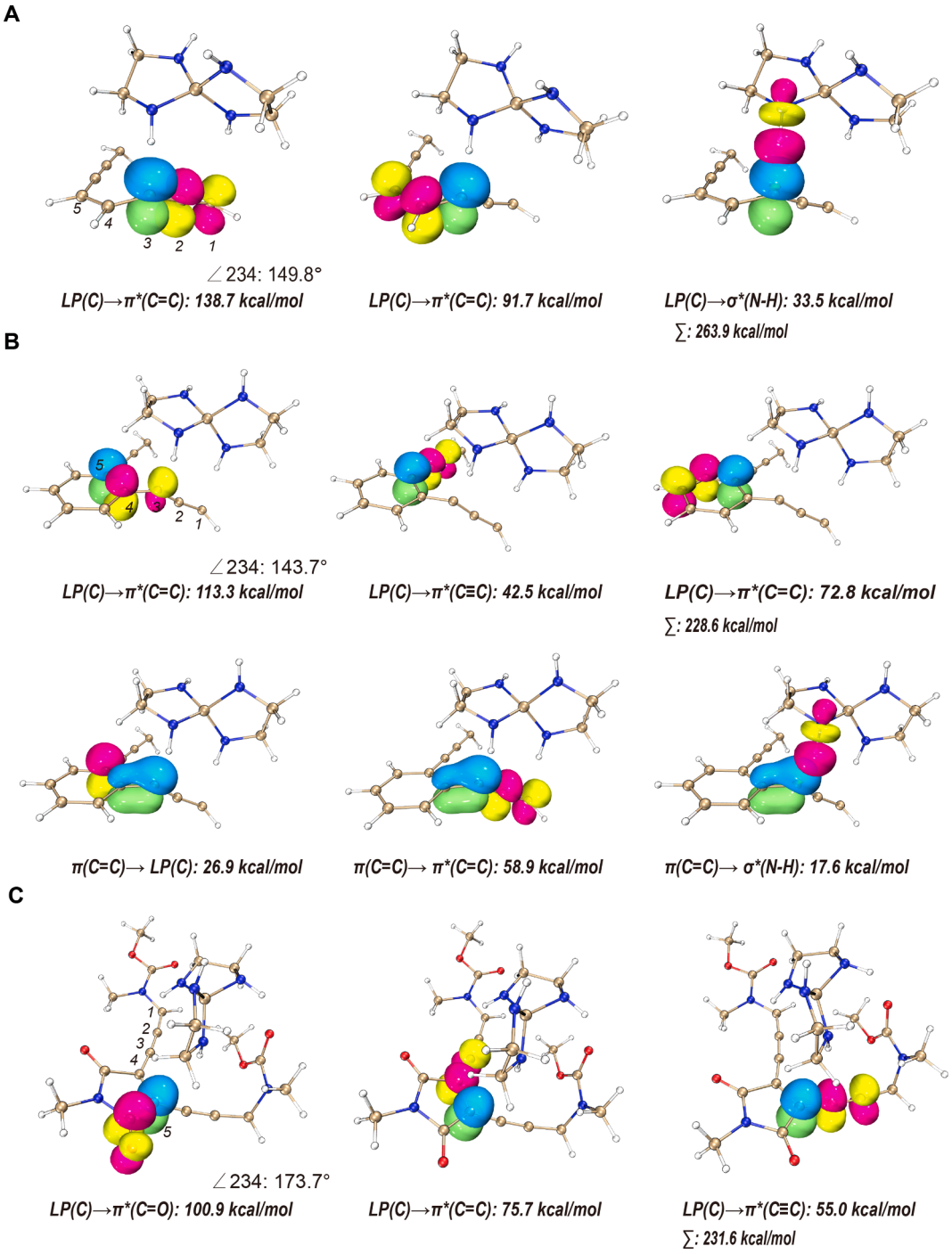

Fig. 4. NBO interactions between the donor orbitals (in cyan and green) and the acceptor orbitals (in magenta and yellow) in the reaction intermediates catalyzed by NPN. (A). **INT1**; (B). **INT2**; (C). **INT3**. The color code is the same as Fig. 3. The substituents at the yne sites are omitted for clarity in **R1** and **R2**. Σ represents the sum of all the NBO interactions in each system. The orbitals are generated at the dens.ity of 0.08 a.u.

still could locate on C5 and buta-1,2,3-triene (C═C═C) substrate in ionic state was sustained because **R3** itself has the ability to stabilize the carbon LP on C5. So ∠234 is almost intact, close to 180°. The deprotonated **R1** and **R2** structures show weaker conjugation of the negative charge compared to **R3**, which is the major cause of the strong orbital interactions produced by the substrates and the protonated NPN. Such interactions with NPN+p are gradually weakened (33.5 and 17.6 kcal/mol in **R1** and **R2** respectively) following the increased stability of EDY-p (**R1** < **R2** < **R3**). In the cases of **R1** and **R2**, the direct n→σ^* interactions between the substrate and the catalyst indicate that the complete separation of the deprotonated substrate and the protonated NPN in the intermediate state is impossible, though the reaction is in a stepwise mode.

In general, the maleimide structure has sufficient ability to stabilize the extra charge, in addition, NPN+p further stabilizes **R3**-p substrate according to van der Waals interactions. Hence, the electronic structure of the charge separated intermediate **INT3** is the most stable (21.4 kcal/mol lower in electronic energy compared to **TS1-R3**, Figure S3). On the contrary, **R1**-p has the weakest ability of charge delocalization, which requires extra stabilization from NPN+p (33.5 kcal/mol according to NBO analysis). The charge separated intermediate is the least stable (3.4 kcal/mol lower in electronic energy compared to **TS1-R1**, Figure S3). The results of **R2** is in between, due to its medium ability of charge delocalization.

The resonance structure suggests that carbon LP located in C3 position in the presence of NPN in **R1**. It is close to sp^2 hybridization whose *p* orbital interacts with two adjacent π^*(C—C) orbitals, resulting in the distortion of ∠234 (149.8°, Fig. 4B). In **R2**, NBO results show the resonance structure of carbon LP on C5 position, producing strong interaction with π^*(C3-C4) orbital (113.3 kcal/mol), which indicates strong

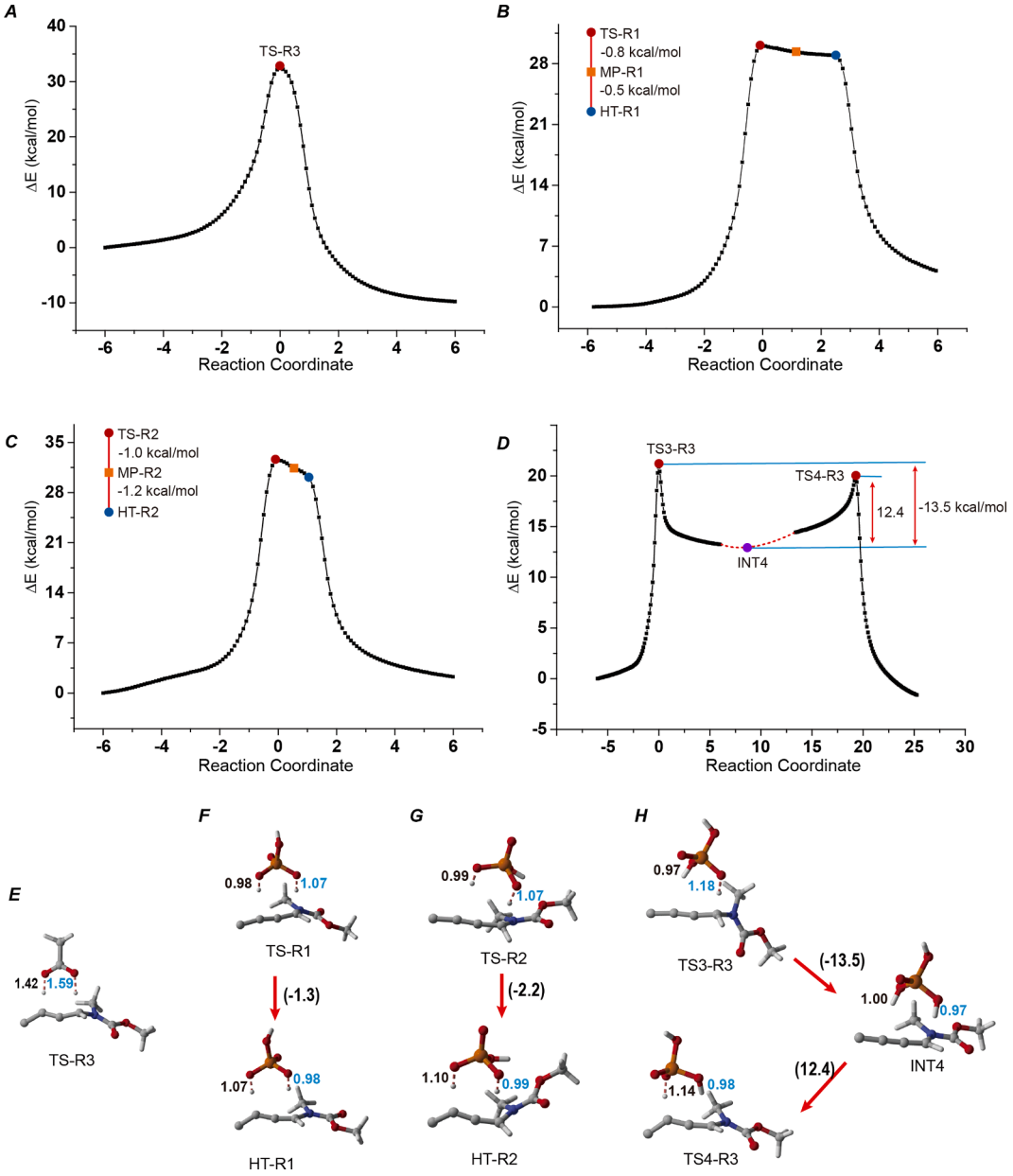

Fig. 5. 1,3-proton transfer potential energy curves and the corresponding structures of **R3** + acetic acid (A and E), **R1** + $H_2PO_4^-$ (B and F), **R2** + $H_2PO_4^-$ (C and G), and **R3** + $H_2PO_4^-$ (D and H).The black lines in the PES are from IRC calculations at B3LYP-D3/6-311+G* with CPCM model of water. Only the reactive sites are shown in the structures with P in orange, N in blue, O in red, C in gray, and H in white. The OH distance in blue represents the proton for abstraction, while the OH distance in black represents the proton for addition (units in Å). The numbers in the parenthesis along the red arrows represent the relative single-point energies corresponding to the PES (units in kcal/mol).

delocalization of the charge density to the reactive C3 site. The electronic density on π(C3-C4) orbital is not evenly distributed so that the interaction between *p* orbital on C3 position and the σ^*(N-H) orbital in the catalyst is enhanced. Such donor-accptor orbital interaction is similar to orbital interactions in metal catalyzed C—H activation [14,57]. In this way, ∠234 is also affected significantly (143.7°, Fig. 4C). The reactivity is confirmed by the frontier orbitals as well (Figure S4). The C5 site of **R2**-p with or without NPN did not show high reactivity due to extremely low HOMO orbital densities, even though it is the location of carbon LP. To this end, we suspect that the structure of **R2**-p has to resonant to recover aromaticity and reactivity to achieve proton addition on C3 position. In the other two EDY structures, reactivities on both C3 and C5 sites are evident in the HOMO orbitals (Figure S4), where direct 1,5-proton transfer might be restrained by C5···H distances in concerted mechanism. Moreover, 1,5-proton transfer in **R3** with the help of CH_3COO^- is possible according to our previous work [21].

For substrates lacking the ability to accommodate the extra negative charge, the reaction mechanism is mainly determined by the catalyst. A stepwise mechanism is only achieved through the orbital interaction between the substrate and the catalyst in the charge separated intermediate; otherwise, it will go through a fully concerted or "hidden-TS" concerted mechanism on the condition that the catalyst could work as proton donor and acceptor simultaneously. Catalysts such as $N(CH_3)_3$, cannot balance the structural instability of **R1** and **R2** after proton abstraction, thus failed to assistant the proton transfer process, while work well in **R3**.

3.3. The potential energy surfaces in water phase

The above analysis provides an impressive picture of how the stability of the charge-separated intermediates in gas phase determines the shape of the PES. In reality, the solvation effect also affects the shape of the PES. Thus the potential energy curves are generated from IRC calculations of the TSs optimized at B3LYP-D3/6-311+G* with CPCM description of water as the solvent. Due to its large polarity, water could provide extra stabilization to the charge separated intermediates. The PES are depicted in Fig. 5. Compared to the PES generated in gas phase (Fig. 2), the solvent slightly changed the shape of the PES. The PES of fully concerted mechanism was less symmetric compared to the one obtained from the gas phase (Fig. 5A). Meanwhile, the solvation effect facilitated the transformation from TS to the hidden-TS in "hidden-TS" concerted mechanism, as the structural changes occurred in a shorter reaction coordinate range (Fig. 5B and C). Besides, the intermediate generated from the stepwise mechanism became more stable due to the solvation effect (Fig. 5D). But most importantly, the reaction mechanism in each specific system and the evolution of the PES depending on both substrate and catalyst still sustained, which suggests that the stability of the structures in gas phase plays the dominant role. For all of the systems examined in this work, only the reaction mechanism of **R3** catalyzed by single water molecule shifted from fully concerted in gas phase to "hidden-TS" concerted mechanism (Figure S6). Such conversion could be attributed to the extra stabilization of the hydronium ion in the solvent, which reconfirms our findings that by stabilizing the charge separated structure in the proton transfer process, it is possible for the PES to evolving from fully concerted mechanism, to "hidden-TS" concerted mechanism, and then to stepwise mechanism.

4. Conclusion

In conclusion, the 1,3-proton transfer process in enediyne systems with different catalysts and substrates are investigated in detail. The potential energy surfaces are revealed to follow three different mechanisms: fully concerted mechanism, "hidden-TS" concerted mechanism and in a stepwise manner depending on the stability of the charge separated intermediate after proton abstraction. NBO analysis shows that the substituents at the ene position have a dramatic effect on the stability of the negatively charged EDY after proton leaving, where the maleimide moiety reveals the strongest NBO interactions to delocalize the carbon lone pair, which is attributed to the significant stabilization of the intermediate. In general, the combination of a stable substrate after deprotonation and a relatively strong base is fundamental to push the reaction in a stepwise direction. For the substrates requiring extra interaction from the catalyst to stabilize the negative charge in the charge separated intermediate, a catalyst serving as proton donor and acceptor is a necessity to achieve successful proton transfer. In fully concerted mechanism, the catalyst plays the vital role. In this case, the catalyst has to satisfy the requirement of working as proton donor and acceptor simultaneously; meanwhile the protonation of the catalyst will reduce its stability, thus the protonation and deprotonation processes are synchronous, while in "hidden-TS" concerted mechanism, it is asynchronous because accepting one extra proton will not affect the catalyst's stability.

The trends uncovered in this work could be applied in other chemical reactions with similar charge separated intermediate. By changing the substituents in the substrate and carefully selecting the catalyst, it is possible to lower the energy of the intermediate and even abort the reaction. Our work provides a strategy to manipulate the potential energy surface, for example, converting a concerted mechanism into a stepwise one, which will help to capture the reaction intermediate and elucidate the reaction mechanism experimentally.

CRediT authorship contribution statement

Hailong Ma: Conceptualization, Validation, Investigation, Data curation, Visualization, Writing - original draft. **Mengsi Zhang:** Investigation, Data curation. **Yaxian Zhang:** Investigation, Data curation. **Aiguo Hu:** Conceptualization, Writing - review & editing. **Yun Ding:** Conceptualization, Writing - review & editing, Supervision, Funding acquisition.

Declaration of Competing Interest

The authors declare that they have no known competing financial interests or personal relationships that could have appeared to influence the work reported in this paper.

Acknowledgement

The authors thank the supports from National Natural Science Foundation of China (21503078) and Natural Science Foundation of Shanghai (20ZR1413400).

Appendix A. Supplementary material

Supplementary data associated with this article can be found, in the online version, at https://doi.org/10.1016/j.cplett.2021.139298.

References

[1] M. Eigen, L. De Maeyer, Self-dissociation and protonic Charge Transport in Water and, Proc. Roy. Soc. London. Series A. Mathe. Phys. Sci. 247 (1958) 505–533.
[2] M. Eigen, Proton Transfer, Acid-Base Catalysis, and Enzymatic Hydrolysis. Part I: Elementary Processes, Angew. Chem. Int. Ed. English 3 (1964) 1–19.
[3] N. Agmon, The Grotthuss Mechanism, Chem. Phys. Lett. 244 (1995) 456–462.
[4] G.A. Voth, Computer Simulation of Proton Solvation and Transport in Aqueous and Biomolecular Systems, Acc. Chem. Res. 39 (2006) 143–150.
[5] A. Hassanali, F. Giberti, J. Cuny, T.D. Kühne, M. Parrinello, Proton Transfer through the Water Gossamer, Proc. Nat. Acad. Sci. 110 (2013) 13723–13728.
[6] D. Marx, Proton Transfer 200 Years after von Grotthuss: Insights from Ab Initio Simulations, ChemPhysChem 7 (2006) 1848–1870.
[7] L. Rodríguez-Santiago, M. Sodupe, A. Oliva, J. Bertran, Intramolecular Proton Transfer in Glycine Radical Cation, J. Phys. Chem. A 104 (2000) 1256–1261.
[8] S.X. Tian, J. Yang, Ab initio Photoionization Dynamics of β-alanine, J. Chem. Phys. 126 (2007) 141103.

[9] S. Xiao, L. Wang, Y. Liu, X. Lin, H. Liang, Theoretical Investigation of the Proton Transfer Mechanism in Guanine-cytosine and Adenine-thymine Base Pairs, J. Chem. Phys. 137 (2012) 195101.

[10] D. Soler-Polo, J.I. Mendieta-Moreno, D.G. Trabada, J. Mendieta, J. Ortega, Proton Transfer in Guanine-Cytosine Base Pairs in B-DNA, J. Chem. Theory Comput. 15 (2019) 6984–6991.

[11] D. Jacquemin, J. Zú niga, A. Requena, J.P. Céron-Carrasco, Assessing the Importance of Proton Transfer Reactions in DNA, Accounts Chem. Res. 47 (2014) 2467–2474.

[12] E.E. Romero, F.E. Hernandez, Solvent Effect on the Intermolecular Proton Transfer of the Watson and Crick Guanine-cytosine and Adenine-thymine Base Pairs: a Polarizable Continuum Model Study, PCCP 20 (2018) 1198–1209.

[13] K.W. Chan, et al., C-H Activation and Proton Transfer Initiate Alkene Metathesis Activity of the Tungsten(IV)-Oxo Complex, J. Am. Chem. Soc. 140 (2018) 11395–11401.

[14] J.J. Gair, Y. Qiu, R.L. Khade, N.H. Chan, A.S. Filatov, Y. Zhang, J.C. Lewis, Synthesis, Characterization, and Theoretical Investigation of a Transition State Analogue for Proton Transfer during C-H Activation by a Rhodium-Pincer Complex, Organometallics 38 (2019) 1407–1412.

[15] S.J. Schmidtke, D.F. Underwood, D.A. Blank, Probing Excited-State Dynamics and Intramolecular Proton Transfer in 1-Acylaminoanthraquinones via the Intermolecular Solvent Response, J. Phys. Chem. A 109 (2005) 7033–7045.

[16] M. Meuwly, A. Bach, S. Leutwyler, Grotthus-Type and Diffusive Proton Transfer in 7-Hydroxyquinoline·$(NH_3)_n$ Clusters, J. Am. Chem. Soc. 123 (2001) 11446–11453.

[17] K.S.A. Peters, Theory-Experiment Conundrum for Proton Transfer, Acc. Chem. Res. 42 (2009) 89–96.

[18] J.J. Park, C.S. Lee, S.Y. Han, Proton Transfer Accounting for Anomalous Collision-Induced Dissociation of Proton-Bound Hoogsteen Base Pair of Cytosine and Guanine, J. Am. Soc. Mass Spectrom. 29 (2018) 2368–2379.

[19] B. Yuan, R. He, W. Shen, M. Li, Effects of Base Strength on the Copper-catalyzed Cycloisomerization of Propargylic Acetates to Form Indolizines: A DFT Study, Tetrahedron 73 (2017) 6092–6100.

[20] B. Yuan, R. He, W. Shen, M. Li, Influence of Base Strength on the Proton-Transfer Reaction by Density Functional Theory, Eur. J. Org. Chem. 2017 (2017) 3947–3956.

[21] M. Zhang, et al., Triggering the Antitumor Activity of Acyclic Enediyne through Maleimide-Assisted Rearrangement and Cycloaromatization, J. Organic Chem. 85 (2020) 9808–9819.

[22] X. You, X. Xie, H. Chen, Y. Li, Y. Liu, Cyano-Schmittel Cyclization through Base-Induced Propargyl-Allenyl Isomerization: Highly Modular Synthesis of Pyridine-Fused Aromatic Derivatives. Chemistry — A, Eur. J. 21 (2015) 18699–18705.

[23] L. Yang, R. Fang, Mechanism of Gold (I)-catalyzed Double Migration-benzannulation Cascade toward Naphthalenes: Deprotonation/Protonation Mediated by Water, J. Mol. Catal. A: Chem. 379 (2013) 197–206.

[24] T.P. Gonçalves, M. Mohamed, R.J. Whitby, H.F. Sneddon, D.C. Harrowven, Exploring Diradical Chemistry: A Carbon-Centered Radical May Act as either an Anion or Electrophile through an Orbital Isomer, Angew. Chem. Int. Ed. 54 (2015) 4531–4534.

[25] B. Yuan, R. He, W. Shen, W. Hu, M. Li, DFT Study on the CuBr-catalyzed Synthesis of Highly Substituted Furans: Effects of Solvent DMF, Substrate MeOH, Trace H_2O and the Metallic Valence State of Cu, RSC Adv. 6 (2016) 20294–20305.

[26] N.E. Smith, W.H. Bernskoetter, N. Hazari, The Role of Proton Shuttles in the Reversible Activation of Hydrogen via Metal-Ligand Cooperation, J. Am. Chem. Soc. 141 (2019) 17350–17360.

[27] J. Chen, P. Yuan, L. Wang, Y. Huang, Enantioselective β-Protonation of Enals via a Shuttling Strategy, J. Am. Chem. Soc. 139 (2017) 7045–7051.

[28] D.V. Vidhani, M.E. Krafft, I.V. Alabugin, Gold(I)-Catalyzed Allenyl Cope Rearrangement: Evolution from Asynchronicity to Trappable Intermediates Assisted by Stereoelectronic Switching, J. Am. Chem. Soc. 138 (2016) 2769–2779.

[29] G. dos Passos Gomes, I.V. Alabugin, Drawing Catalytic Power from Charge Separation: Stereoelectronic and Zwitterionic Assistance in the Au(I)-Catalyzed Bergman Cyclization, J. Am. Chem. Soc. 139 (2017) 3406–3416.

[30] K.C. Nicolaou, W.-M. Dai, Chemistry and Biology of the Enediyne Anticancer Antibiotics, Angew. Chem. Int. Ed. English 30 (1991) 1387–1416.

[31] C.-Y. Chang, X. Yan, I. Crnovcic, T. Annaval, C. Chang, B. Nocek, J.D. Rudolf, D. Yang, Hindra, G. Babnigg, A. Joachimiak, G.N. Phillips, B. Shen, Resistance to Enediyne Antitumor Antibiotics by Sequestration, Cell Chem. Biol. 25 (2018) 1075–1085.e4.

[32] R.R. Jones, R.G. Bergman, p-Benzyne. Generation as an intermediate in a thermal isomerization reaction and trapping evidence for the 1,4-benzenediyl structure, J. Am. Chem. Soc. 94 (1972) 660–661.

[33] R.G. Bergman, Reactive 1,4-Dehydroaromatics, Acc. Chem. Res. 6 (1973) 25–31.

[34] B. König, W. Pitsch, M. Klein, R. Vasold, M. Prall, P.R. Schreiner, Carbonyl- and Carboxyl-Substituted Enediynes: Synthesis, Computations, and Thermal Reactivity, J. Organic Chem. 66 (2001) 1742–1746.

[35] M.D. Lee, et al., Calichemicins, a Novel Family of Antitumor Antibiotics. 2. Chemistry and Structure of Calichemicin γ_1^I, J. Am. Chem. Soc. 109 (1987) 3466–3468.

[36] R.K. Mohamed, P.W. Peterson, I.V. Alabugin, Concerted Reactions That Produce Diradicals and Zwitterions: Electronic, Steric, Conformational, and Kinetic Control of Cycloaromatization Processes, Chem. Rev. 113 (2013) 7089–7129.

[37] A.G. Myers, E.Y. Kuo, N.S. Finney, Thermal Generation of α,3-Dehydrotoluene from (Z)-1,2,4-Heptatrien-6-yne, J. Am. Chem. Soc. 111 (1989) 8057–8059.

[38] A.G. Myers, P.S. Dragovich, Design and dynamics of a chemically triggered reaction cascade leading to biradical formation at subambient temperature, J. Am. Chem. Soc. 111 (1989) 9130–9132.

[39] K. Saito, T. Watanabe, K. Takahashi, [4+2]-Type Cycloadditions of Tropone and Heptafulvene Derivatives with a Tautomeric Mixture of Cycloheptatrienylidene and Cycloheptatetraene, Chem. Lett. 18 (1989) 2099–2102.

[40] M.J. Frisch, G.W. Trucks, H.B. Schlegel, G.E. Scuseria, M.A. Robb, J.R. Cheeseman, G. Scalmani, V. Barone, G.A. Petersson, H. Nakatsuji, X. Li, M. Caricato, A. Marenich, J. Bloino, B.G. Janesko, R. Gomperts, B. Mennucci, H.P. Hratchian, J.V. Ortiz, A.F. Izmaylov, J.L. Sonnenberg, D. Williams-Young, F. Ding, F. Lipparini, F. Egidi, J. Goings, B. Peng, A. Petrone, T. Henderson, D. Ranasinghe, V.G. Zakrzewski, J. Gao, N. Rega, G. Zheng, W. Liang, M. Hada, M. Ehara, K. Toyota, R. Fukuda, J. Hasegawa, M. Ishida, T. Nakajima, Y. Honda, O. Kitao, H. Nakai, T. Vreven, K. Throssell, J.A. Montgomery, Jr., J.E. Peralta, F. Ogliaro, M. Bearpark, J. J. Heyd, E. Brothers, K.N. Kudin, V.N. Staroverov, T. Keith, R. Kobayashi, J. Normand, K. Raghavachari, A. Rendell, J.C. Burant, S.S. Iyengar, J. Tomasi, M. Cossi, J.M. Millam, M. Klene, C. Adamo, R. Cammi, J.W. Ochterski, R.L. Martin, K. Morokuma, O. Farkas, J.B. Foresman, D.J. Fox, Gaussian 09 Revision E.01. Gaussian, Inc., Wallingford, CT, 2016.

[41] S. Chen, B. Huang, S. Sun, Y. Ding, A. Hu, Unexpected [2+2] Photocycloaddition between Enediyne Compounds in Solid State, Asian J. Organic Chem. 6 (2017) 775–779.

[42] H. Lu, et al., Facilitating Myers-Saito Cyclization through Acid-triggered Tautomerization for the Development of Maleimide-based Antitumor Agents, J. Mater. Chem. B 8 (2020) 1971–1979.

[43] V. Barone, M. Cossi, Quantum Calculation of Molecular Energies and Energy Gradients in Solution by a Conductor Solvent Model, J. Phys. Chem. A 102 (1998) 1995–2001.

[44] M. Cossi, N. Rega, G. Scalmani, V. Barone, Energies, structures, and electronic properties of molecules in solution with the C-PCM solvation model, J. Comput. Chem. 24 (2003) 669–681.

[45] S. Grimme, J. Antony, S. Ehrlich, H. Krieg, A Consistent and Accurate Ab Initio Parametrization of Density Functional Dispersion Correction (DFT-D) for the 94 Elements H-Pu, J. Chem. Phys. 132 (2010) 154104.

[46] K. Fukui, The path of chemical reactions - the IRC approach, Acc. Chem. Res. 14 (1981) 363–368.

[47] J.P. Foster, F. Weinhold, Natural Hybrid Orbitals, J. Am. Chem. Soc. 102 (1980) 7211–7218.

[48] A.E. Reed, F. Weinhold, Natural Bond Orbital Analysis of Near-Hartree-Fock Water Dimer, J. Chem. Phys. 78 (1983) 4066–4073.

[49] A.E. Reed, R.B. Weinstock, F. Weinhold, Natural Population Analysis, J. Chem. Phys. 83 (1985) 735–746.

[50] A.E. Reed, L.A. Curtiss, F. Weinhold, Intermolecular Interactions from a Natural Bond Orbital, Donor-Acceptor Viewpoint, Chem. Rev. 88 (1988) 899–926.

[51] E.D. Glendening, A.E. Reed, J.E. Carpenter, F. Weinhold, NBO Version 3.1.

[52] W. Humphrey, A. Dalke, K. Schulten, VMD: Visual Molecular Dynamics, J. Mol. Graph. 14 (1996) 33–38.

[53] T. Lu, F. Chen, Multiwfn: A Multifunctional Wavefunction Analyzer, J. Comput. Chem. 33 (2012) 580–592.

[54] G. dos Passos Gomes, A.E. Morrison, G.B. Dudley, I.V. Alabugin, Optimizing Amine-Mediated Alkyne-Allene Isomerization to Improve Benzannulation Cascades: Synergy between Theory and Experiments, Eur. J. Org. Chem. 2019 (2019) 512–518.

[55] F.-Q. Shi, X. Li, Y. Xia, L. Zhang, Z.-X. Yu, DFT Study of the Mechanisms of In Water Au(I)-Catalyzed Tandem [3,3]-Rearrangement/Nazarov Reaction/[1,2]-Hydrogen Shift of Enynyl Acetates: A Proton-Transport Catalysis Strategy in the Water-Catalyzed [1,2]-Hydrogen Shift, J. Am. Chem. Soc. 129 (2007) 15503–15512.

[56] M. Zhang, et al., Experimental and Computational Study on the Intramolecular Hydrogen Atom Transfer Reactions of Maleimide-Based Enediynes After Cycloaromatization, J. Organic Chem. 86 (2021) 1549–1559.

[57] Y. Sun, H. Tang, K. Chen, L. Hu, J. Yao, S. Shaik, H. Chen, Two-State Reactivity in Low-Valent Iron-Mediated C-H Activation and the Implications for Other First-Row Transition Metals, J. Am. Chem. Soc. 138 (2016) 3715–3730.